Journal of Alloys and Compounds 509 (2011) 7688–7691

Contents lists available at ScienceDirect

Journal of Alloys and Compounds

journal homepage: www.elsevier.com/locate/jallcom

Mo microalloying effect on the glass-forming ability, magnetic, mechanical and corrosion properties of $(Fe_{0.76}Si_{0.096}B_{0.084}P_{0.06})_{100-x}Mo_x$ bulk glassy alloys

Xue Li[a,*], Chunling Qin[b], Hidemi Kato[a], Akihiro Makino[a], Akihisa Inoue[c]

[a] Institute for Materials research, Tohoku University, Katahira 2-1-1, Sendai 980-8577, Japan
[b] School of Materials Science and Engineering, Hebei University of Technology, Tianjin 300132, China
[c] Tohoku University, Katahira 2-1-1, Sendai 980-8577, Japan

ARTICLE INFO

Article history:
Received 17 December 2010
Received in revised form 14 April 2011
Accepted 15 April 2011
Available online 23 April 2011

Keywords:
Bulk glassy alloy
Glass-forming ability
Magnetism and corrosion resistance

ABSTRACT

The effect of Mo addition on the glass-forming ability (GFA), magnetic properties, mechanical properties and corrosion resistance of $(Fe_{0.76}Si_{0.096}B_{0.084}P_{0.06})_{100-x}Mo_x$ (x = 0, 2, 4 and 6 at.%) bulk glassy alloys (BGAs) with high Fe contents was investigated. The 2 at.% Mo addition makes the alloy composition approach towards a eutectic point, which could result in an increase in the GFA. The BGA rod with diameters up to 3.5 mm was produced by copper mold casting. These BGAs exhibit a rather high saturation magnetization of 0.98–1.51 T and lower coercive force of 1.7–2.1 A/m. A significant improvement in corrosion resistance was observed with microalloying Mo element in 1 N H_2SO_4 solution. Furthermore, these Fe-based BGAs show super-high strength of ~3.3 GPa and Young's modulus of 200 GPa.

1. Introduction

Since the finding of glass transition before crystallization in Fe-based amorphous alloys, followed by the synthesis of Fe–(Al, Ga)–(P, C, B) BGAs [1,2], many kinds of Fe-based ferromagnetic BGA systems have been developed as soft-magnetic materials [3,4]. Now, Fe-based bulk glassy alloys (BGAs) have attracted specific attention due to not only their unique combination of excellent magnetic properties, high fracture strength, high hardness and good corrosion resistance, but also the low cost resulting from plentiful natural resources of Fe element on the earth [5–10]. Although Ponnambalam et al. [11] and Lu et al. [12] reported BGAs with critical diameters up to 12 mm by addition of small amounts of Y or Er to previously reported Fe–Cr–Mo–B–C BGAs [9], those alloys exhibit paramagnetic properties at room temperature and the problem of extremely brittleness has been unresolved. The corrosion resistance of Fe-based BGAs have been investigated by Pang et al. in $Fe_{75-x-y}Cr_xMo_yC_{15}B_{10}$ and $Fe_{43}Cr_{16}Mo_{16}(C, B, P)_{25}$ systems [9,13]. However, those investigations were concentrated on the subject of improving the corrosion resistance, the Fe content was remarkably decreased to as low as 30 at.% due to addition of large amounts of corrosion resistant Cr and Mo elements. As a result, the magnetic moments of those Fe-based BGAs disappear at room temperature, and those alloys became non-ferromagnetic materials. Therefore, it is necessary to develop Fe-based ferromagnetic BGAs with unusual combination of high GFA, high saturation magnetization and good corrosion resistance for applications as ferromagnetic materials using under the severe environments.

Recently, minor alloying techniques have obviously shown beneficial effects on both GFA and properties for some Fe-based metallic glasses [14–17]. In this paper, based on $Fe_{76}Si_{9.6}B_{9.6}P_{4.8}$ BGA [18,19] with high GFA leading to the glassy rods with diameters up to 2.5 mm, the effect of Mo addition on the GFA, magnetic, mechanical, and corrosion properties was studied. It was found that the addition of small amounts of Mo element is very effective in enlarging the GFA and improving corrosion resistance for the Fe-based BGAs, though Mo element slightly decreases the magnetic properties of the alloys.

2. Experimental

Multi-component $(Fe_{0.76}Si_{0.096}B_{0.084}P_{0.06})_{100-x}Mo_x$ (x = 0, 2, 4, and 6 at.%) alloy ingots were prepared by induction melting under a high purified argon atmosphere using the elements with high purity of Fe (99.9 mass%), Mo (99.95 mass%), B (99.9 mass%), and Si (99.99 mass%). P was alloyed by adding prealloyed Fe–15.6 mass% P ingots. This prealloy was also prepared by induction melting and exhibited the purities of 99.9 mass%. Their compositions are nominally expressed in atomic percentage. Cylindrical rods with diameters up to 3.5 mm and a length of 40 mm were also fabricated under a high purified argon atmosphere by copper mold casting. The glassy alloy ribbons with a cross section of 0.02 mm × 1 mm were prepared by melt-spinning.

The glassy structure was examined by X-ray diffraction (XRD) with Cu-K_α radiation. The thermal stability associated with glass transition temperature (T_g), crystallization temperature (T_x), and supercooled liquid region ($\Delta T_x = T_x - T_g$) was examined by a differential scanning calorimetry (DSC) at a heating rate of 0.67 K/s. Sample morphology was observed by scanning electron microscopy (SEM). The melting (T_m) and liquidus (T_l) temperatures were measured with a differential

* Corresponding author.
E-mail address: lixue@imr.tohoku.ac.jp (X. Li).

0925-8388/$ – see front matter © 2011 Elsevier B.V. All rights reserved.
doi:10.1016/j.jallcom.2011.04.081

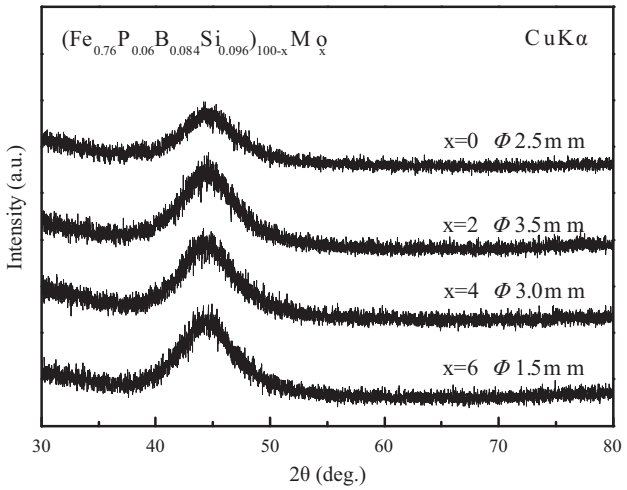

Fig. 1. XRD patterns of $(Fe_{0.76}Si_{0.096}B_{0.084}P_{0.06})_{100-x}Mo_x$ (x = 0, 2, 4, and 6 at.%) glassy alloy rods.

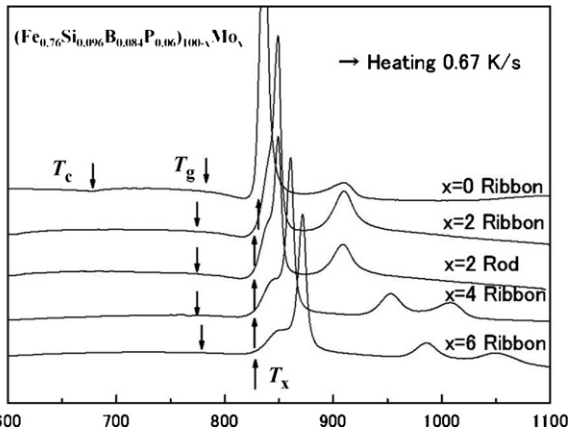

Fig. 2. The DSC traces of the $(Fe_{0.76}Si_{0.096}B_{0.084}P_{0.06})_{100-x}Mo_x$ glassy alloy ribbons (x = 0, 2, 4, and 6 at.%) and rod (x = 2 at.%, ϕ 3.5 mm).

thermal analyzer (DTA) at a heating rate of 0.067 K/s. Magnetic properties, saturation magnetization (J_s) and coercive force (H_c), were measured with a vibrating sample magnetometer (VSM) under an applied field of 400 kA/m and a B–H loop tracer under a field of 800 A/m, respectively. Compressive tests were performed on Instron testing machine at a strain rate of 5×10^{-4} at room temperature using glassy rods with a dimension of 2 mm in diameter and 4 mm in length. Corrosion resistance of the alloys was evaluated by electrochemical measurements in 1 N H_2SO_4 solution open to air at room temperature. Prior to electrochemical measurements, the specimens were polished mechanically with SiC paper up to grit 1500 in cyclohexane, degreased in acetone, washed in distilled water, dried in air, and further exposed to air for 24 h for good reproducibility. Electrochemical measurements were conducted in a three-electrode cell using a platinum counter electrode and an Ag/AgCl reference electrode. Potentiodynamic polarization curves were measured at a potential sweep rate of 50 mV/min after open-circuit immersion for about 20 min when the open-circuit potential became almost steady.

3. Results and discussion

The Mo content not more than 6 at.% was selected in this study in order to obtain a rather high J_s value, since J_s decreases with decreasing Fe content. Firstly, we examined the effect of additional element Mo on glass formation of the Fe–Si–B–P–Mo alloys. Fig. 1 shows XRD patterns of the as-cast $(Fe_{0.76}Si_{0.096}B_{0.084}P_{0.06})_{100-x}Mo_x$ (x = 0, 2, 4 and 6 at.%) rods with critical diameters of 1.5–3.5 mm. All the diffraction patterns consist only of a broad peak and no any appreciable crystalline peaks are seen for all the rod samples, indicating that a glassy single structure is formed in the investigated compositional range. The outer surface is very smooth and neither concave nor ruggedness due to a crystalline phase is observed for these bulk samples.

The critical diameters (D_{cr}) for glass formation for the $(Fe_{0.76}Si_{0.096}B_{0.084}P_{0.06})_{100-x}Mo_x$ (x = 0, 2, 4 and 6 at.%) alloys are 2.5 mm, 3.5 mm. 3.0 mm and 1.5 mm for x = 0, 2, 4 and 6 at.%, respectively, summarized in Table 1. It is seen that the GFA of the alloys is enhanced with the addition of Mo element and reaches the maximum at 2 at.% Mo.

Fig. 2 shows DSC curves of the $(Fe_{0.76}Si_{0.096}B_{0.084}P_{0.06})_{100-x}Mo_x$ (x = 0, 2, 4, and 6 at.%) glassy alloys produced by melt spinning. Each DSC traces exhibit distinct glass transition, followed by a supercooled liquid region and then crystallization. In Table 1, we can see that the glass transition temperature (T_g) and crystallization temperature (T_x) decrease with alloying Mo element to the Fe–Si–B–P glassy alloys and almost keep constant with a further increase in Mo content of the alloys. At the same time, the supercooled liquid region ($\Delta T_x = T_x - T_g$) increases with the addition of Mo element. The minor addition of 2 at.% Mo to the alloy causes an extension of ΔT_x from 49 K for the alloy without Mo element to 55 K for $(Fe_{0.76}Si_{0.096}B_{0.084}P_{0.06})_{98}Mo_2$. Therefore, it can be concluded that the microalloying Mo element to Fe–Si–B–P glassy alloys is effective for increasing the thermal stability of the supercooled liquid phase. A larger supercooled liquid region and a higher stability of the supercooled liquid phase are useful for the superplastic processing of these alloys in supercooled liquid state to produce various intricate devices. A DSC trace for $(Fe_{0.76}Si_{0.096}B_{0.084}P_{0.06})_{98}Mo_2$ rod sample with a diameter of 3.5 mm was also shown in Fig. 2. It was found that the DSC trace of the rod sample was almost same with that of the ribbon sample, indicating the same glassy structure.

In order to understand beneficial effects of the alloying element Mo on GFA, the melting behavior of the $(Fe_{0.76}Si_{0.096}B_{0.084}P_{0.06})_{100-x}Mo_x$ (x = 0, 2, 4 and 6 at.%) alloys were investigated by DTA at a heating rate of 0.067 K/s, as shown in Fig. 3. It is found that almost only one endothermic peak appears in the curve for each alloy of x = 0–4, although two or three endothermic peaks may partly overlap together, but two clear endothermic peaks appear in the curve for x = 6 alloy. These results imply that the compositions of x = 0–4 alloys lie in the vicinity of a eutectic point and the composition of x = 6 alloy has deviated from the eutectic point. The 2 at.% Mo-containing alloy analogously exhibits only one exothermic peak and has the lowest T_l and the narrowest temperature interval between T_m and T_l. Therefore, the $(Fe_{0.76}Si_{0.096}B_{0.084}P_{0.06})_{98}Mo_2$ alloy is considered to be the closest to the deep eutectic point among the alloys. Table 1 summarizes the thermal parameters of $(Fe_{0.76}Si_{0.096}B_{0.084}P_{0.06})_{100-x}Mo_x$ (x = 0, 2, 4 and 6 at.%) alloys. The $T_{rg}(=T_g/T_l)$ and γ $(=T_x/(T_g+T_l))$ values slightly increase with the addition of 2 at.% Mo to the alloy and

Table 1
The glass transition temperature (T_g), the crystallization temperature (T_x), the critical diameter (D_{cr}), the parameters for GFA (ΔT_x, T_g/T_l and γ), and magnetic properties (J_s, H_c) for the Fe-based BGAs $(Fe_{0.76}Si_{0.096}B_{0.084}P_{0.06})_{100-x}Mo_x$ (x = 0, 2, 4, and 6 at.%).

Composition	T_g (K)	T_x (K)	ΔT_x (K)	T_g/T_l	γ	J_s (T)	H_c (A/m)	D_{cr} (mm)
x = 0	783	832	49	0.571	0.386	1.51	1.7	2.5
x = 2	773	828	55	0.572	0.389	1.35	1.9	3.5
x = 4	773	827	54	0.560	0.384	1.10	1.9	3.0
x = 6	776	827	51	0.538	0.373	0.98	2.1	1.5

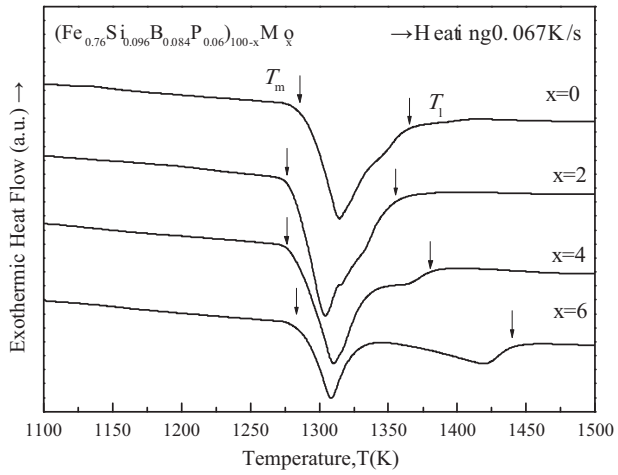

Fig. 3. DTA curves of $(Fe_{0.76}Si_{0.096}B_{0.084}P_{0.06})_{100-x}Mo_x$ (x = 0, 2, 4, and 6 at.%) glassy alloy ribbons.

then decrease with further increasing Mo content. The large ΔT_x, high T_{rg} and γ value are simultaneously obtained for the alloys with microalloying Mo content up to 4 at.%, which is the reason for the success of forming the glassy rods with large diameters of 3.0–3.5 mm.

The magnetic, mechanical and corrosion properties of these Fe-based glassy alloy rods were further measured. Fig. 4 shows VSM traces of glassy alloy ribbons $(Fe_{0.76}Si_{0.096}B_{0.084}P_{0.06})_{100-x}Mo_x$ (x = 0, 2, 4, and 6 at.%). The $(Fe_{0.76}Si_{0.096}B_{0.084}P_{0.06})_{100-x}Mo_x$ (x = 0, 2, 4 and 6 at.%) BGAs possess good soft-magnetic properties, as shown in Fig. 4. The J_s decreases from 1.51 T for the alloy without Mo to 0.98 T for the 6 at.% Mo added alloy. The alloy ribbons subjected to annealing for 300 s at 50 K under T_g have the low H_c of 1.7–2.1 A/m.

Fig. 5 shows compressive stress–strain curves of $(Fe_{0.76}Si_{0.096}B_{0.084}P_{0.06})_{100-x}Mo_x$ (x = 0, 2, 4, and 6 at.%) BGA rods with a diameter of 1.5 mm. Initially, the curves behave like typical Fe-based BGAs, exhibiting an elastic strain of about 2% at yield strength of 3300 MPa and Young's modulus of 200 GPa for $(Fe_{0.76}Si_{0.096}B_{0.084}P_{0.06})_{98}Mo_2$ alloy. The plastic strain of 0.7% for the alloy without Mo decreases with increasing in the Mo content. The alloy with microalloying 2 at.% Mo still exhibits a small extent of plastic strain (~0.3%), whereas $(Fe_{0.76}Si_{0.096}B_{0.084}P_{0.06})_{96}Mo_4$ and $(Fe_{0.76}Si_{0.096}B_{0.084}P_{0.06})_{94}Mo_6$ glassy alloys with higher Mo content are subjected to full brittle fracture.

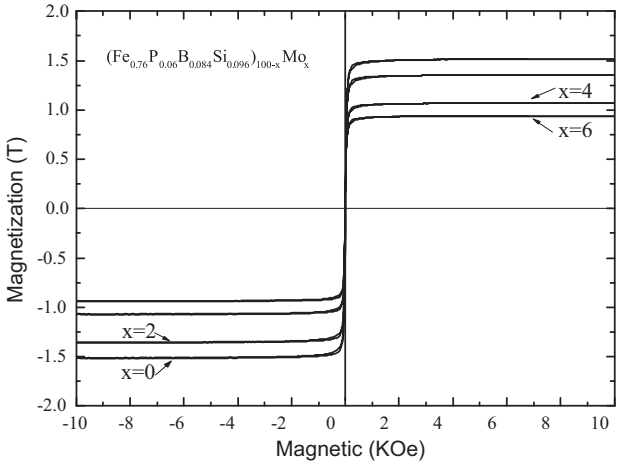

Fig. 4. VSM traces of glassy alloy ribbons $(Fe_{0.76}Si_{0.096}B_{0.084}P_{0.06})_{100-x}Mo_x$ (x = 0, 2, 4, and 6 at.%).

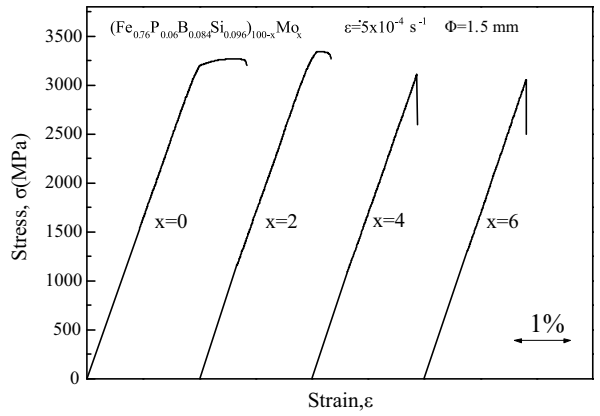

Fig. 5. Compressive stress–strain curves of $(Fe_{0.76}Si_{0.096}B_{0.084}P_{0.06})_{100-x}Mo_x$ (x = 0, 2, 4, and 6 at.%) BGA rods with a diameter of 1.5 mm.

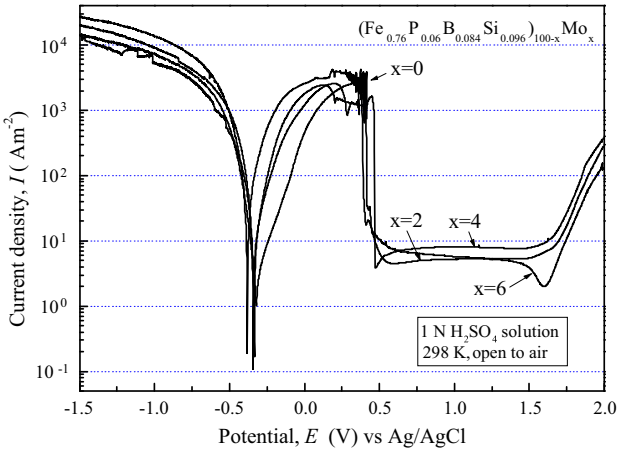

Fig. 6. Potentiodynamic polarization curves of the $(Fe_{0.76}Si_{0.096}B_{0.084}P_{0.06})_{100-x}Mo_x$ (x = 0, 2, 4, and 6 at.%) glassy alloy rods in diameters of 1.5 mm in 1 N H_2SO_4 solution open to air at 298 K.

The corrosion resistance was conducted by electrochemical measurements. Fig. 6 shows the potentiodynamic polarization curves of the as-cast $(Fe_{0.76}Si_{0.096}B_{0.084}P_{0.06})_{100-x}Mo_x$ (x = 0, 2, 4 and 6) BGA rods with a diameter of 1.5 mm in 1 N H_2SO_4 solution open to air at 298 K. The as-cast $Fe_{76}Si_{9.6}B_{9.6}P_{4.8}$ alloy dissolves actively and its anodic current density increases quickly by anodic polarization. In addition, the stable polarization curve with increasing potential of above 0.6 V vs. Ag/AgCl cannot be obtained, because the sample suffers a severe damage by the further anodic polarization. However, the significant improvement in corrosion resistance is observed with alloying Mo element to the Fe–Si–B–P alloy. All the Mo-containing alloys exhibit a wide passive region in 1 N H_2SO_4 solution. From their curves, we can see that the glassy alloys containing different amount of Mo content show similar corrosion behavior in this solution. This indicates that only microalloying 2 at.% Mo can remarkably enhance the corrosion resistance of the Fe-based alloys in H_2SO_4 solution. XPS analysis revealed that the high corrosion resistance of Mo-containing glassy alloys is attributed to the formation of Mo-enriched surface film during immersion in 1 N H_2SO_4 solution.

4. Conclusions

A ferromagnetic bulk $(Fe_{0.76}Si_{0.096}B_{0.084}P_{0.06})_{100-x}Mo_x$ (x = 0, 2, 4, and 6 at.%) glassy alloys with critical diameters in the range up

to 3.5 mm was developed by copper mold casting. The addition of a small amount of Mo is found to be effective in enhancing the glass-forming ability and corrosion resistance. This Fe-based ferromagnetic bulk glassy alloy system exhibits a rather high saturation magnetization of 0.98–1.51 T and high compressive strength. The corrosion resistance of the alloys is highly improved with alloying Mo elements. All the Mo-containing alloys exhibit wide passive region by anodic polarization in 1 N H_2SO_4. Among them, the Fe-based BGAs with microalloying 2 at.% Mo demonstrates the best combination of high GFA, good soft-magnetic properties, high strength as well as good corrosion resistance, and is promising for future applications as structural and functional materials applied under the severe environmental conditions.

Acknowledgement

This work was supported by Global COE Program 'Materials Integration (International Center of Education and Research), Tohoku University.

References

[1] A. Inoue, J.S. Gook, Mater. Trans. JIM 36 (1995) 1180–1183.
[2] A. Inoue, Y. Shinohara, J.S. Gook, Mater. Trans. JIM 36 (1995) 1427–1433.
[3] T.D. Shen, R.B. Schwarz, Appl. Phys. Lett. 75 (1999) 49–51.
[4] A. Inoue, A. Takeuchi, B.L. Shen, Mater. Trans. JIM 42 (2001) 970–978.
[5] A. Inoue, Acta Mater. 48 (2000) 279–306.
[6] A. Inoue, B.L. Shen, Mater. Trans. JIM 43 (2002) 766–769.
[7] B.L. Shen, M. Akiba, A. Inoue, Intermetalllics 15 (2007) 655–658.
[8] A. Inoue, B.L. Shen, C.T. Chang, Acta Mater. 52 (2004) 4093–4099.
[9] S.J. Pang, T. Zhang, K. Asami, A. Inoue, Acta Mater. 50 (2002) 489–497.
[10] B.L. Shen, M. Akiba, A. Inoue, J. Appl. Phys. 100 (2006) 043523.
[11] V. Ponnambalam, S.J. Poon, G.J. Shiflet, J. Mater. Res. 19 (2004) 1320–1323.
[12] Z.P. Lu, C.T. Liu, J.R. Thompson, W.D. Porter, Phys. Rev. Lett. 92 (2004) 245503.
[13] S.J. Pang, T. Zhang, K. Asami, A. Inoue, J. Mater. Res. 17 (2002) 701–704.
[14] X. Li, C.T. Chang, T. Kubota, C.L. Qin, A. Makino, A. Inoue, Mater. Trans. 49 (2008) 2887–2890.
[15] A. Makino, X. Li, K. Yubuta, C.T. Chang, T. Kubota, A. Inoue, Scripta Mater. 60 (2009) 277–280.
[16] X. Li, A. Makino, K. Yubuta, H. Kato, A. Inoue, Mater. Trans. 50 (2009) 1286–1289.
[17] X. Li, K. Yubuta, A. Makino, A. Inoue, Mater. Sci. Eng. A 527 (2010) 2598–2602.
[18] A. Makino, T. Kubota, C.T. Chang, M. Makabe, A. Inoue, Mater. Trans. JIM Vol. 48 (2007) 3024–3027.
[19] A. Makino, T. Kubota, M. Makabe, C.T. Chang, A. Inoue, Mater. Sci. Eng. B 148 (2007) 166–170.